BiVO4 Fern Architectures: A Competitive Anode for Lithium-Ion Batteries

Deepak P. Dubal,*[a, b] Deepak R. Patil,[c] Santosh S. Patil,[d] N. R. Munirathnam,[c] and

Pedro Gomez-Romero* [b]

[a] Dr. D. P. Dubal School of Chemical Engineering, The University of Adelaide Adelaide, South Australia 5005 (Australia) E-mail: dubaldeepak2@gmail.com

[b] Dr. D. P. Dubal, Prof. P. Gomez-Romero Catalan Institute of Nanoscience and Nanotechnology (ICN2) The Barcelona Institute of Science and Technology (CSIC-BIST) Campus UAB, Bellaterra, 08193 Barcelona (Spain) E-mail: dubaldeepak2@gmail.com pedro.gomez@icn2.cat

[c] Dr. D. R. Patil, Prof. N. R. Munirathnam Centre for Materials for Electronics Technology Department of Electronics and Information Technology (DeitY) Goverment of India, Pune 411008 (India)

[d] Dr. S. S. Patil Department of Physics, Chonnam National University Gwangju 500–757 (Republic of Korea)

ABSTRACT

The development of high-performance anode materials for lithium-ion batteries (LIBs) is currently subject to much interest. In this study, BiVO4 fern architectures are introduced as a new anode material for LIBs. The BiVO4 fern shows an excellent reversible capacity of 769 mAhg -1 (ultrahigh volumetric capacity of 3984 mAhcm-3) at 0.12 A g-1 with large capacity retention. A LIB full cell is then assembled with a BiVO4 fern anode and LiFePO4 (LFP, commercial) as cathode material. The device can achieve a capacity of 140 mAhg -1 at 1C rate, that is, 81% of the capacity of the cathode and maintained to 104 mAhg -1 at a high rate of 8C, which makes BiVO4 a promising candidate as a high-energy anode material for LIBs.

Introduction

Battery performance depends not only on the properties of the anode and cathode electrode materials but also on interfacial and surface effects. Therefore, the development of suitable anode and cathode materials with superior interface and surface properties along with stability and low cost are in high demand. To keep up with the recent rapid advancement in cathode materials, suitable and innovative high-performance anode materials are urgently required. Generally, lithiated graphite (LiC6) has been used as an anode material from last two and half decades due to its low cost, sheer abundance, nontoxicity, and outstanding kinetics. [1] However, graphite suffers from low theoretical capacity (372 mAhg -1) and safety problems arising from lithium dendrite formation, which limit their large-scale application. [1,2] The potential of Li+ intercalation into graphite is around 0 V, whereby Li dendrites form and cause the short circuit of batteries. Moreover, the volume change of carbonaceous materials causes cracks, resulting in lower capacity. [2] As an alternative, transition metal oxides (TMOs), with density twice that of graphite, exhibit a twofold enhancement in volumetric energy density, which is crucial for advanced applications.[3,4] Certain TMOs, such as Fe3O4 , Co3O4 , Li4Ti5O12, SnO2, TiO2 , Na2Ti3O7 , have thus been effectively employed as anodes that showed higher theoretical capacities for Li storage, as well as good cycling stability and safety. Recently, vanadium-based oxides such as V2O5 , Li3VO4 , LiV3O8 , and LiV2O5 , have been widely used as anodes for LIBs due to their natural abundance, low toxicity, and improved safety. [2,5,6] Many of these vanadates consist of double chains of VO6 octahedra with metal cations in the interlayer space that facilitate the intercalation/deintercalation of Li ions, leading to high capacity, extended voltage and superior kinetics.[5,6] Among them, Li3VO4 has been extensively investigated due to its excellent electrochemical properties, such as high capacity (323 mAhg -1) and good reversibility. [7–9] In addition, FeVO4 a has recently emerged as a promising anode material for Li-ion batteries with a theoretical capacity of 847 mAhg -1 (5.4 mol Li per mol FeVO4).[10] For example, Yan et al. investigated FeVO4 nanorods as LIB anode material and achieved a

reversible discharge capacity of 527 mAhg -1 at a current rate of 75 mAg -1 (see the Supporting Information, Table S1).[11] BiVO4 has been extensively studied in photocatalysis and we very recently reported its use in supercapacitors.[12,13] In the present investigation, for the first time, we have tested BiVO4 as an anode material for LIBs. The motivation to use BiVO4 in LIBs is its unique layered crystal structure, as well as the inclusion of multivalent Bi and V. The layered structure of monoclinic BiVO4 can facilitates the intercalation/de-intercalation of Li ions to a greater extent than other dense bulk materials, which is of relevance in the field of rechargeable LIBs.[14] The only investigation to date on BiVO4 as a cathode in primary Li-ion cell was reported by Pasquali and Pistoia in 1989.[15] To our knowledge, no further investigation on BiVO4 as LIB anode has since been performed. Thus, it is worth investigating the electrochemical properties of BiVO4 as an anode for LIBs to understand the fundamental chemistry of the cell reactions. From the morphological point of view, typical fern-like hyperbranched morphology of BiVO4 presented herein has attracted widespread attention, particularly for electrochemical and catalytic applications, since these structures exhibit remarkable connectivity among crystals.[16] In this study, BiVO4 fern architectures were extensively characterized to investigate their physicochemical and electrochemical properties. Finally, as a proof of concept, we have assembled and tested a full LIB cell with LiFePO4 as a cathode and the BiVO4 fern architecture as an anode. Results and Discussion The phase determination of hydrothermally synthesized BiVO4 powder was confirmed by X-ray diffraction (XRD) with Rietveld refinement (Figure 1 a). For Rietveld refinement, the FullProf Suite program with VESTA graphical interface was used. The Rietveld plot suggests a perfect match between experimental and simulated XRD patterns (R-factor=7%). The initial structural parameters were taken from an earlier report.[17] The lattice parameters obtained from the refinement are a=7.2558 A, b=11.7091 A, c=5.0964 A, and beta=134.248° which are consistent with reported values.[17] From the crystal structure, it is seen that the unit cell of BiVO4 is composed of a BiO8 dodecahedron and a VO4 tetrahedron in which similar metal atoms are connected to each other in a continuous zigzag manner (Figure 1 a, inset). Moreover, since the Bi and V atoms are alternately arranged along the crystallographic c axis, BiVO4 exhibits the characteristics ofa layered structure that is feasible for Li ion storage. Furthermore, the oxidation states of Bi and V in BiVO4 were

investigated by X-ray photoelectron spectroscopy (XPS; Figure 1 b, c). The magnified Bi4f spectrum shows two peaks at binding energies of 159.3 eV and 164.5 eV, suggesting that Bi is in +3 oxidation state (Figure 1 b). The Bi4f5/2 and Bi4f7/2 peaks are well resolved with spin–orbit splitting of 5.32 eV. Similarly, the V 2p spectrum exhibits two peaks at binding energies of 516.9 eV (V2p3/2) and 524.4 eV (V2p1/2), indicating that V is in the +5 oxidation state.[18,19] The morphological features, size, and crystal structure were evaluated by FE-SEM (field-emission scanning electron microscopy) and high-resolution transmission electron microscopy (HR-TEM) analysis. The FE-SEM images of as-prepared BiVO4 sample (Figure 2 a, b) indicate typical fern-like hyper-branched morphology which has attracted a wide attention particularly for electrochemical and catalysis applications since these structures exhibit a remarkable connectivity among crystals. Generally, fern architectures consist of several small branches densely packed together with sufficiently high porosity to afford facile access of electrolyte ions. Submicron-sized BiVO4 fern architectures are composed of an intact backbone with a number of small branches symmetrically connected from both sides (Figure 2 a, b). The length of the backbone is about 8 to 10 mm, whereas the length of the branches is 0.4–1 mm (Figure S1). Under hydrothermal reaction conditions, continuous rotation of particles takes place by Brownian motion to generate branch-like structures. Further growth of these branches occurs by Ostwald ripening and leads to structures that are adjust to minimize the total surface free energy. [20] Consequently, as-formed small branch structures act as a building blocks for the growth and development of BiVO4 fern architectures. Previous reports have claimed that an isotropic growth of branches along the [001] direction accounts for the development of BiVO4 fern/dendrite structures.[20] Figure 2 c–f shows TEM and HR-TEM images of BiVO4 and the associated selective area electron diffraction (SAED) pattern. The TEM images are consistent with the FE-SEM results, showing submicron-sized fern architectures with several sub-branches with lengths of 0.4–1 mm and diameters of 100–400 nm. Figure 2 e shows the HR-TEM image of BiVO4 sample with well-ordered lattice fringes with interplanar distances of 5.82 a corresponding to the (002) crystal plane of monoclinic BiVO4 . The SAED pattern (Figure 2 f) shows regular bright spots indicating good crystallinity of the as-synthesized monoclinic BiVO4 sample.

As mentioned above, monoclinic BiVO4 has had great success in photocatalytic applications. Here, for the first time we have tested BiVO4 as an anode material for Li-ion battery application. In this regard, we tested the BiVO4 electrode's electrochemical performance in a half-cell configuration with Li metal as both counter and reference electrode. Some electrochemical insights are provided by cyclic voltammetry measurements (Figure 3 a). The CV curves strongly indicate contributions from two materials; the Bi-based anode and the Li3VO4 electrode.[21,22] The CV curve in the initial cycle shows four reduction peaks at around 1.94, 1.64, 0.88, and 0.52 V, corresponding to the intercalation/de-intercalation processes of Li ions in BiVO4 . The first peak at 1.94 V can be assigned to the decomposition of the electrolyte and the formation of the solid–electrolyte interface (SEI),[23] whereas the peaks at 1.64 V and 0.88 V might be associated to the formation of metallic Bi and the reduction of V5+ to V 4+ , respectively. In the case of the cathodic peak at 0.52 V, there are two possibilities. It might be due to the reduction of V 4+ to V 3+ and or to the reaction between Li and Bi to form Li3Bi alloy. [21,22] Interestingly, in the subsequent cycle, the peak at 0.52 V splits into two peaks at around 0.49 and 0.71 V, which are attributed to the reduction of V 4+ to V 3+ and formation of Li3Bi, respectively. [21,22] In the first anodic cycle, three oxidation peaks at about 0.96, 1.42, and 2.74 V are clearly observed. Among which, the peaks at 0.96 and 1.42 V are attributed to the dealloying of Bi and the oxidation of V 3+ to V 5+ , respectively, whereas the anodic peak at 2.74 corresponds to the oxidation of metallic Bi. Unsurprisingly, the peaks at 1.64 V in the cathodic scan and 2.74 V in the anodic scan disappeared in subsequent cycles, owing to their irreversible nature. However, the redox peaks corresponding to Bi alloying/dealloying (cathodic 0.71 V/ anodic 0.96 V), as well as redox transitions of V (0.88 and 0.49 V, cathodic, and 1.37– 1.64 V, anodic), are extremely reversible for the next cycles.[22–24] Thus, this unique material can provide two charge storage mechanisms—alloying/dealloying and faradaic redox transitions—and is expected to provide high capacity. The galvanostatic charge–discharge (GCD) curves further show similar trends like CV measurements. Figure 3 b shows the first few GCD curves of BiVO4 electrodes in half cell configuration measured at 1.1 Ag -1 . As indicated, during the first cycle, a large irreversible capacity of 1543 mAhg -1 is obtained, associated to the SEI layer at the BiVO4 electrode with

Columbic efficiency of 67.2%, which is common to all battery anodes. The complete reaction of BiVO4 with Li should involve 6 Li ions according to the Equation (1):

$$BiVO4 + 6\ Li^{+} \rightarrow Li3Bi + Li3VO4 \quad (1)$$

Based on this reaction, the theoretical capacity can be calculated as 662 mAhg -1 . In the subsequent cycle, the discharge capacity was found to be 1024 mAhg -1 , which keeps decreasing for next few cycles and obtained a stable discharge capacity of 676 mAhg -1 after 7th cycle, suggesting comparable or even better performance than other vanadates (Table S1).[25–28] This discharge capacity can be translated to an excellent volumetric capacity of 3515 mAhcm-3 , considering the high bulk density of 5.2 gmcm-3 . The initial decrease in discharge capacity can be attributed to the activation of the electrode material, as well as to decomposition of the electrolyte and formation of an SEI on the electrode. The rate capability of BiVO4 at different current densities from 0.12 to 11.45 A g-1 was investigated. Notably, the BiVO4 shows excellent Li-ion storing capability and cycling stability even at high rates. The reversible capacity is found to be 769 mAhg -1 (3984 mAhcm-3) at 0.12 A g-1 , (Figure 3 c). It should be noted that even at a high current density of 11.45 A g-1 the material can still present a reversible capacity of 340 mAhg -1 (1774 mAhcm-3), which is still a very substantial value (about 91% of the theoretical capacity of graphite) indicating a high rate performance. Moreover, BiVO4 achieve a capacity of 571 mAhg -1 after changing the current density to 1.1 A g-1 after 90 cycles at various current densities, which signifies an excellent rate capability. Figure 3 d shows the cycling performance of the BiVO4 anode at 1.1 Ag -1 over 200 cycles, indicating an extraordinary charge–discharge cycling stability with negligible capacity loss. Significantly, the Coulombic efficiency of the BiVO4 electrodes is maintained above 80% in the beginning and stabilized at 97% over 200 cycles (Figure S2). This exceptional long-term stability may be ascribed to the unique dendrite-like morphology, which acts to buffer the volume expansion during charging and discharging, whereas the alloying mechanism maintains the high capacity for longterm cycling. The Li-ion charge kinetics were further analyzed by

estimating the capacitive and diffusion controlled charge contributions to the total charges stored by the BiVO4 electrode.[29] For this analysis, the CV curves were measured at different scan rates for BiVO4 electrodes in half-cell design (Figure S2). The slope of the corresponding log(v) vs. log(i) plot (Figure 4 a) is 0.68 for the cathodic peak and is consistent with kinetics dominated by a diffusion-controlled process. The total charge stored in the BiVO4 electrode (Qt) is the sum of the surface capacitive charge (Qc) and the diffusion-controlled charge (Qd), which can be expressed as Equation (2):

$$Q_t = Q_c + Q_d \quad (2)$$

The capacitive contribution Qc is associated with surface adsorption, as well as surface redox reactions, and hence is scanrate independent. However, semi-infinite linear diffusion is assumed for the diffusion processes and thus Qd varies according to the reciprocal square root of the scan rate, hence the Equation (2) can be rewritten as Equation (3):

$$Q_t = Q_c + k\nu^{-1/2} \quad (3)$$

where k is a constant and Qc can be determined by plotting Qt against the reciprocal of the square root of scan rate. Figure 4 b shows the percent contribution of separate capacitive and diffusion-controlled charge contributions measured at different scan rates. The analysis suggests that about 62% of the total charge stored by the BiVO4 electrode is contributed by diffusion-controlled processes at 1 mV s-1 . Moreover, at a high scan rate of 5 mV s-1 , the capacitive and diffusion charge contributions are almost equal (i.e., 49% and 51%, respectively), whereas at a high scan rate of 10 mVs -1 , the capacitive charge is 78% due to the faster charge kinetics. Thus, the significant diffusion-controlled charge contribution is attributed to the conversion reactions during the Li interaction. The Li-ion diffusion coefficient in the BiVO4 electrode was further estimated by the Randles–Sevick equation [Eq. (4)]:[27]

$$i_p = 2.69 \times 10^5 n^{3/2} A D_{Li}^{1/2} \nu^{1/2} C \quad (4)$$

where ip is the current maximum in amps (we considered current value at 3 points), n is the number of electrons involved in charge storage, A is the electrode area in cm2 (for simplicity we have considered geometrical area), DLi is the diffusion coefficient in cm2 s -1 , n is the scan rate in V s-1 , and C is the concentration of Li-ion in mol cm-3 . The diffusion coefficients for BiVO4 calculated at different peak currents is in the range of 10-9 cm2 s -1 for different scan rates (Figure 4 c) which are greater than the values reported for other vanadates.[26,27,30] The diffusion coefficients for BiVO4 increase with increasing scan rate, further confirming the high rate capability of the material. To investigate the structural reversibility of BiVO4 upon Li insertion/de-insertion, we conducted ex situ XRD measurements on the electrodes by disassembling the coin cells at different charge–discharge states (Figure 4 d). The two intense peaks at 43.58 and 50.58 are the diffraction peaks of the copper current collector. During the first discharge, the ex situ XRD pattern measured at 1.8 V suggests the transformation of pure monoclinic BiVO4 structure into amorphous with weak and broad peaks at around 228 and 278 that corresponds to Li3VO4 (pink circle) [7] and metallic Bi (green stars), respectively (Figure 4 d). As the lithiation process proceeded, the intensity of the two aforementioned peaks increased and two new peaks emerged at around 388 and 398, which are related to the alloying of metallic Bi with lithium, confirming formation of Li3Bi.[15,31] In the next step, upon charging, the changes in the XRD pattern of the electrode underwent reversal to that of the discharged structure and the new phase peaks decreased. In ex situ XRD measured at 2.1 V during charging, that the peaks related to Li3Bi lose their intensities, indicating de-alloying and Li-extraction processes. At the complete charge state (3.0 V), all the peaks are seen to have disappeared and an amorphous materials is formed. Thus, the ex situ XRD analysis is clearly in accordance with the CV and GCD results explained in the previous section. More insights about the change in oxidation states of Bi and V during discharging/charging are investigated by ex situ XPS (Figure S3). Upon first discharge, the Bi4f peaks are shifted to the lower binding energies such as 156.5 eV and 162.3 eV with spin orbit splitting of 5.6 eV, corresponding to metallic Bi (Bi0). Interestingly, in the next charging step this metallic Bi (Bi0) returns to the original Bi 3+ state, suggesting excellent reversibility. Likewise, magnified V 2p XPS spectra suggests the transition of V 5+ to V 3+ and then from V 3+ to V 5+ upon discharging and charging. As a proof of concept,

we assembled a LIB full cell with BiVO4 ferns as the anode and LiFePO4 (LFP, commercial) as the cathode material. Prior to fabrication, the BiVO4 is pre-activated with Li metal foil to eliminate the initial capacity loss by conducting ten complete charge–discharge cycles and paired with LFP. Figure 5 a shows, charge–discharge curves of LFP at 1C rate (1C=170 mAg -1). The LFP exhibits a high specific charge value of 158 mAhg -1 (ca. 93% of the theoretical capacity of 170 mAhg -1) at 1 C rate. Figure 5b shows the comparative charge–discharge curves for BiVO4 and LFP electrodes in halfcell configuration. The charge–discharge curves of a BiVO4 // LFP full cell at different C rates are displayed in Figure 5 c. Interestingly, the device could achieve a capacity of 140 mAhg -1 at 1C rate, which is 81% that of the cathode, and maintained to 104 mAhg -1 at a high C rate of 8C. The full cell gives rise to an average charge and discharge potential at around 3.0 and 2.3 V, respectively. The cycling performance of the full cell was investigated at 1C rate over 100 cycles (Figure 5 d). They present good cycling stability during charge–discharge with a slight capacity loss (around 9%) after 100 cycles. These results suggest the successful implementation of BiVO4 ferns as an anode material for LIBs. The cell performance can be further improved by optimizing the electrode microstructure.

Conclusions

Layered BiVO4 with a high volumetric capacity has been developed as a new anode material. It was easily prepared by a direct hydrothermal method. Ex situ XRD was used to systematically analyze the electrochemical processes. The unique electrode made of BiVO4 fern-like architecture exhibits a high capacity of 769 mAhg -1 (3984 mAhcm-3) at 0.12 A g-1 . As a proof of concept, a BiVO4 //LiFePO4 full cell device was assembled, which achieved capacity of 140 mAhg -1 at 1C rate (81% the capacity of the cathode). This work demonstrates that the BiVO4 holds great promise as a high-energy anode material for lithium-ion batteries.

Experimental Section

Preparation of BiVO4 fern architectures

BiVO4 fern architectures were synthesized by a facile one-pot surfactant-free hydrothermal method, as reported for our previous investigation.[13] First, the reaction solvent was prepared by using diluting conc. HNO3 (5 mL) in distilled H2O (65 mL). This solvent was divided into two equal portions in two separate beakers. Bi(NO3)3 ·5H2O, (2.25 mmol, 98.5%; SDFCL) was dissolved in 35 mL of the solvent. Similarly, NH4VO3 (2.25 mmol, 99%; Fisher Scientific) was also dissolved in 35 mL of solvent. Subsequently the Bi (NO3)3 ·5H2O solution was added dropwise to the solution of NH4VO3 under stirring at room temperature. Then, ammonia solution (25%; Qualigen Chemicals Ltd.) was slowly added until a precipitate formed and the solution maintained a pH ca.7. This reaction mixture was stirred for a further 10 min. Finally, the reaction mixture, including the precipitate, was transferred to a Teflon reactor, fitted into a stainless-steel autoclave and kept in an oven at 180°C for 24 h. The reactor was allowed to cool to room temperature after reaction. The crude material obtained was washed thoroughly with deionized water (100 mL) and ethanol (100 mL), dried at 60°C for 3 h in an oven, and used for further characterization and application.

Materials characterization

X-ray diffraction (XRD-D8, AdvancedBruker-AXS) using CuKa radiation (l=1.5406 nm) was used for phase determination. Surface structures were investigated by using FE-SEM (FEI Quanta 650F Environmental SEM). The TEM and HR-TEM analysis was performed by using Tecnai G2 F20 S-TWIN HR(S) TEM (FEI). X-ray photoelectron spectroscopy (XPS) was carried out obtained by using a PHOIBOS 150 spectrometer (SPECS, Germany).

Preparation of electrode materials and electrochemical testing

Electrodes were prepared by mixing the active material (BiVO4), Super-P conductive carbon black, and polyvinylidene fluoride binder (PVDF) in N-methyl-2-pyrrolidone (NMP) with a 80:10:10 weight ratio. The resulting paste was uniformly coated onto Cu foil, dried at 100°C for 12 h, and pressed under a hydraulic press. The mass loading of BiVO4 was around 2.1 mgcm-2 . A Swageloktype cell was fabricated with BiVO4 and Li metal as working and counter electrodes. A glass fiber and 1m lithium hexafluorophosphate in a 1:1 ethylene carbonate/dimethyl carbonate mixture were used as the separator and electrolyte, respectively. The BiVO4 anode were measured within 3.0 to 0.01 V (vs. Li/Li+) by using a Biologic potentio-galvanostat

Acknowledgement

D.P.D. acknowledges support from the University of Adelaide, Australia for a Research Fellowship grant (VC Fellow) through the Research for Impact Scheme. D.P.D. and P.G.R. acknowledge partial support from the Spanish Ministerio MINECO (Grant MAT2015-68394-R, MINECO/FEDER) and AGAUR (Generalitat de Catalunya) for Project NESTOR (Nanomaterials for Energy STORage) 2014_SGR_1505. D.R.P. would like to thank the Department of Science and Technology (DST) INSPIRE faculty program and Department of Electronics and Information Technology (DeitY, New Delhi) for financial support (IFA13/MS05).

Conflict of interest

The authors declare no conflict of interest.

References

[1] a) M. Armand, J. M. Tarascon, Nature 2008, 451, 652; b) D. P. Dubal, O. Ayyad, V. Ruiz, P. Gjmez-Romero, Chem. Soc. Rev. 2015, 44, 1777.

[2] L. Jiang, Y. Qu, Z. Ren, P. Yu, D. Zhao, W. Zhou, L. Wang, H. Fu, ACS Appl. Mater. Interfaces 2015, 7, 1595 – 1601.

[3] Q. Xia, H. Zhao, Z. Du, Z. Zhang, S. Li, C. Gao, J. Mater. Chem. A 2016, 4, 605– 611.

[4] A. R. Armstrong, C. Lyness, P. M. Panchmatia, M. S. Islam, P. G. Bruce, Nat. Mater. 2011, 10, 223 – 229.

[5] L. Bai, J. Zhu, X. Zhang, Y. Xie, J. Mater. Chem. A 2012, 22, 16957 – 16963.

[6] Y. L. Cheah, V. Aravindan, S. Madhavi, ACS Appl. Mater. Interfaces 2012, 4, 3270 – 3277.

[7] H. Q. Li, X. Z. Liu, T. Y. Zhai, D. Li, H. S. Zhou, Adv. Energy Mater. 2013, 3, 428– 432.

[8] a) Y. Shi, J. Z. Wang, S. L. Chou, D. Wexler, H. J. Li, K. Ozawa, H. K. Liu, Y. P. Wu, Nano Lett. 2013, 13, 4715 – 4720; b) Y. Shi, J. Gao, H. D. Abruna, H. J. Li, H. K. Liu, D. Wexler, J. Z. Wang, Y. Wu, Chem. Eur. J. 2014, 20, 5608 – 5612.

[9] W. T. Kim, Y. U. Jeong, Y. J. Lee, Y. J. Kim, J. H. Song, J. Power Sources 2013, 244, 557 – 560.

[10] D. H. Sim, X. Rui, J. Chen, H. Tan, T. M. Lim, R. Yazami, H. H. Hng, Q. Yan, RSC Adv. 2012, 2, 3630 – 3633.

[11] N. Yan, Y. X. Hongjun, L. W. Chen, Mater. Lett. 2016, 165, 223– 226.

[12] S. S. Patil, D. P. Dubal, V. G. Deonikar, M. S. Tamboli, J. D. Ambekar, P. Gomez-romero, S. S. Kolekar, B. B. Kale, D. R. Patil, ACS Appl. Mater. Interfaces 2016, 8, 31602 –31610.

[13] S. S. Patil, D. P. Dubal, M. S. Tamboli, J. D. Ambekar, S. S. Kolekar, P. Gomez-romero, B. B. Kale, D. R. Patil, J. Mater. Chem. A 2016, 4, 7580 – 7584.

[14] M. R. Palac&n, Chem. Soc. Rev. 2009, 38, 2565 – 2575.

[15] M. Pasquali, G. Pistoia, J. Power Sources 1989, 27, 29 –34.

[16] Y. Zhao, Y. Xie, X. Zhu, S. Yan, S. Wang, Chem. Eur. J. 2008, 14, 1601 – 1606.

[17] Z. Zhao, Z. Li, Z. Zou, Phys. Chem. Chem. Phys. 2011, 13, 4746 – 4753.

[18] S. Liu, K. Yin, W. Ren, B. Cheng, J. Yu, J. Mater. Chem. 2012, 22, 17759 – 17767.

[19] L. Ge, Mater. Chem. Phys. 2008, 107, 465– 470.

[20] L. Zhou, W. Wang, H. Xu, Cryst. Growth Des. 2008, 8, 728– 733.

[21] L. L. Zhou, S. Y. Shen, X. Peng, L. N. Wu, Q. Wang, C. H. Shen, T. T. Tu, L. Huang, J. T. Li, S. G. Sun, ACS Appl. Mater. Interfaces 2016, 8, 23739 – 23745.

[22] Y. Li, M. A. Trujillo, E. Fu, B. Patterson, L. Fei, Y. Xu, S. Deng, S. Smirnov, H. Luo, J. Mater. Chem. A 2013, 1, 12123 – 12127.

[23] H. Su, Y. F. Xu, S. C. Feng, Z. G. Wu, X. P. Sun, C. H. Shen, J. Q. Wang, J. T. Li, L. Huang, S. G. Sun, ACS Appl. Mater. Interfaces 2015, 7, 8488 – 8494.

[24] S. Ni, J. Zhang, J. Ma, X. Yang, L. Zhang, J. Power Sources 2015, 296, 377.

[25] C. Liao, Q. Zhang, T. Zhai, H. Li, H. Zhou, Energy Storage Mater. 2017, 7, 17 .

[26] L. Chen, X. Jiang, N. Wang, J. Yue, Y. Qian, J. Yang, Adv. Sci. 2015, 2, 1500090.

[27] L. Shen, S. Chen, J. Maier, Y. Yu, Adv. Mater. 2017, 29, 1701571.

[28] C. Zhang, C. Liu, X. Nan, H. Song, Y. Liu, C. Zhang, G. Cao, ACS Appl. Mater. Interfaces 2016, 8, 680.

[29] Z. Chen, V. Augustyn, X. Jia, Q. Xiao, B. Dunn, Y. Lu, ACS Nano 2012, 6, 4319.

[30] Y. Yang, J. Li, D. Chen, J. Zhao, J. Electrochem. Soc. 2017, 164, A6001.

[31] D. Su, S. Dou, G. Wang, Nano Energy 2015, 12, 88.

Figures

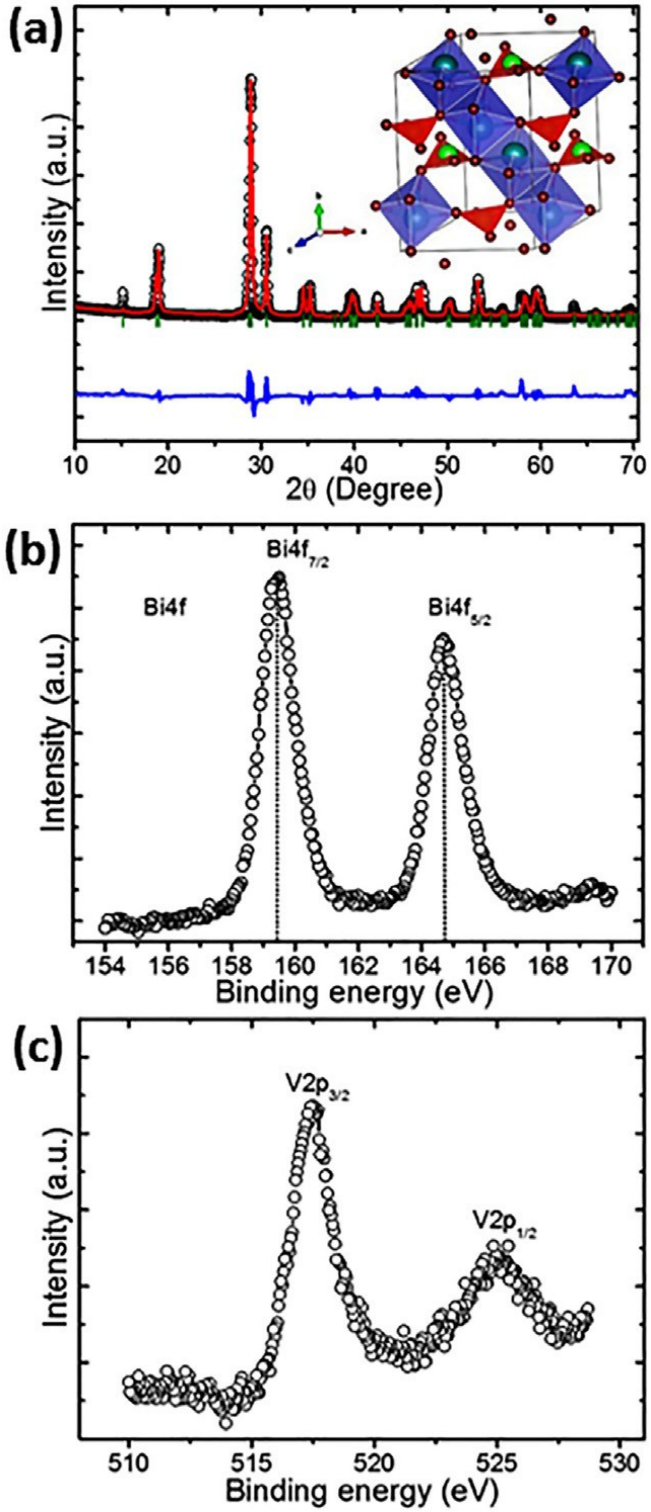

Figure 1. a) Rietveld-refined XRD pattern of BiVO4 fern architecture. Inset shows the crystal structure of monoclinic clinobisvanite BiVO4 with polyhedron structure (VO4 tetrahedron in red,

and BiO8 dodecahedron in light blue). b, c) Core-level XPS spectra for Bi 4f and V2p, respectively.

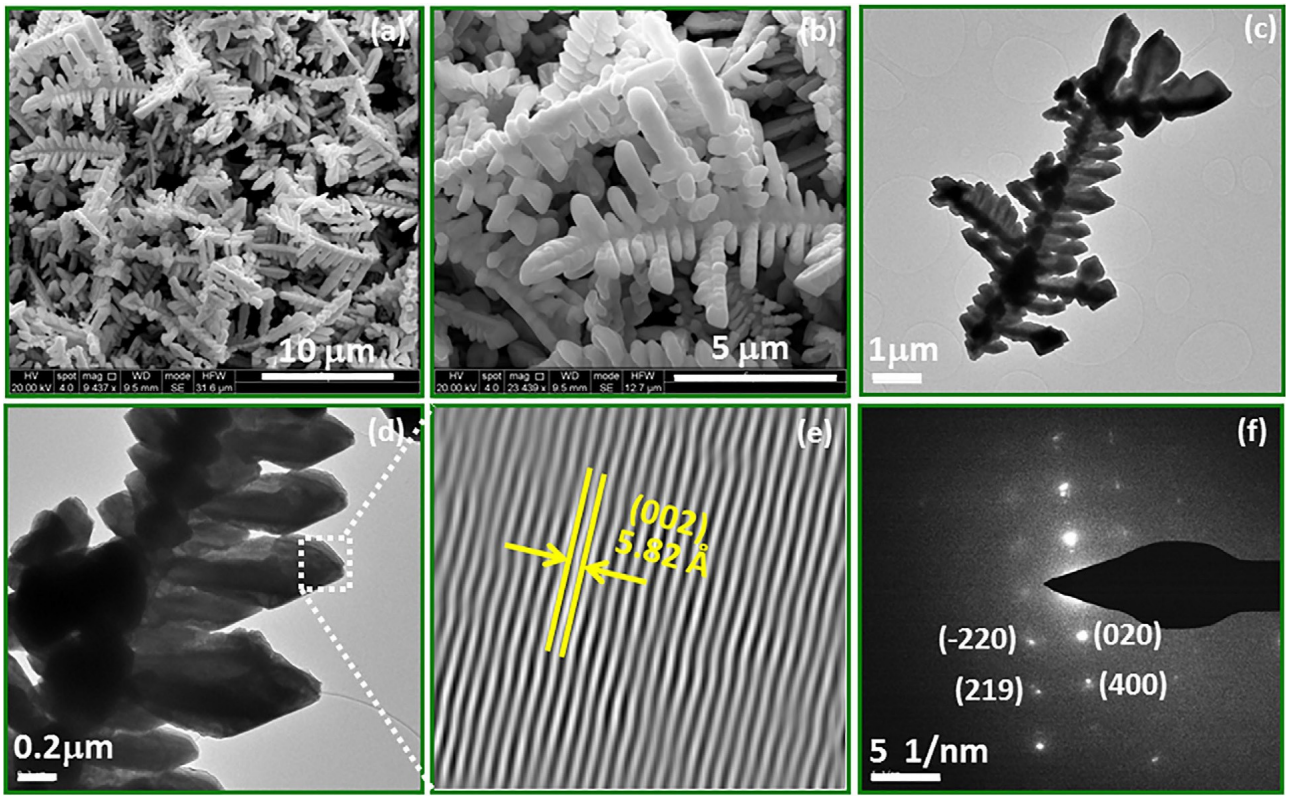

Figure 2. a, b) SEM and c) TEM images of BiVO4 ferns. d) HR-TEM image of a single branch of BiVO4 fern with corresponding inverse fast Fourier Transform (FFT) image of the selected area shown by a white rectangle. e) SAED pattern for BiVO4 sample.

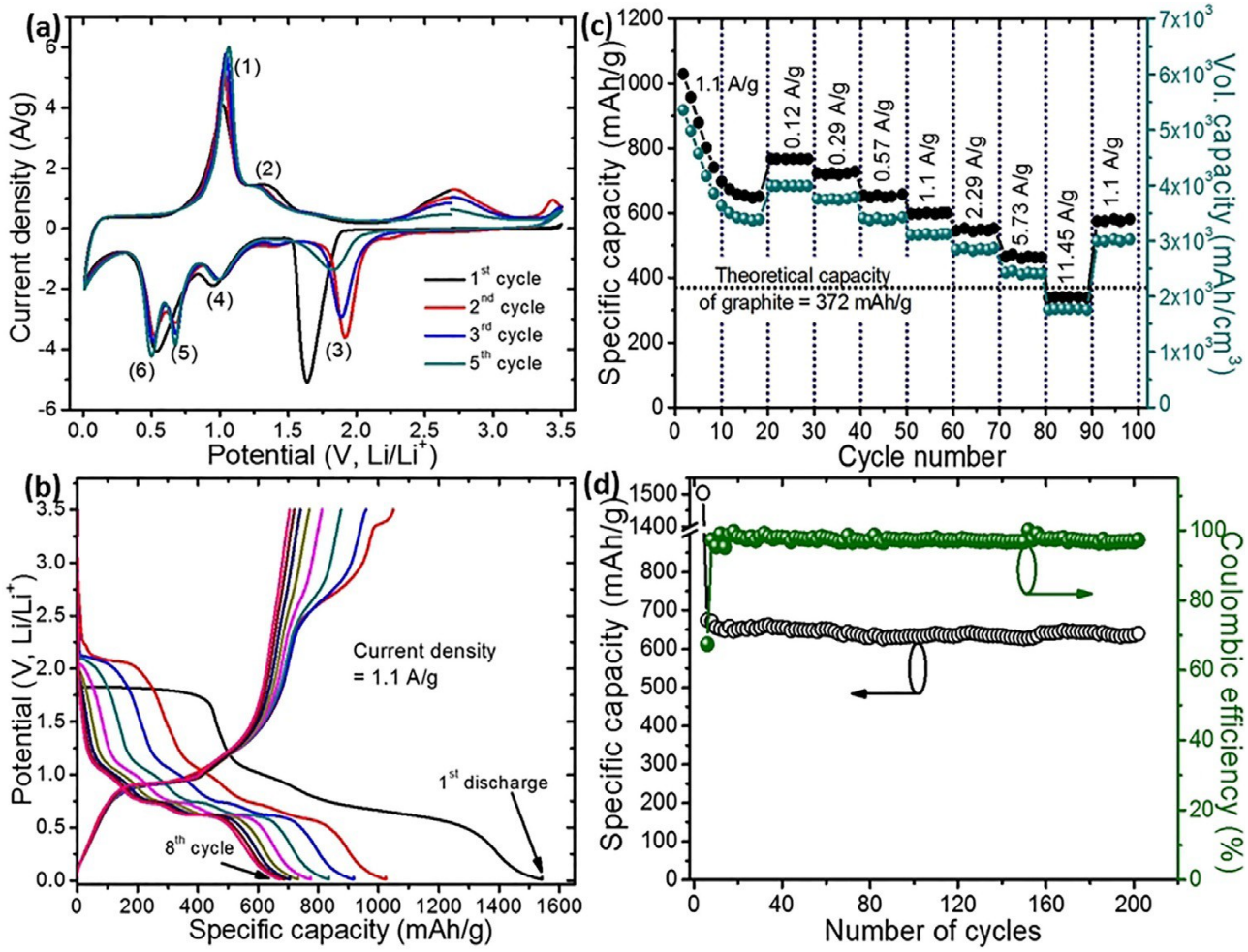

Figure 3. Electrochemical properties of BiVO4 ferns in Li-half cell configuration: a) First few cyclic voltammetry (CV) curves measured at 1 mVs-1 scan rate. b) Initial eight charge–discharge curves measured at 1.1 Ag-1. c) Variation of specific and volumetric capacities with number of cycles at different current densities. d) Cycling stability and Coulombic efficiency over 200 cycles at 1.1 Ag-1, showing excellent capacity retention.

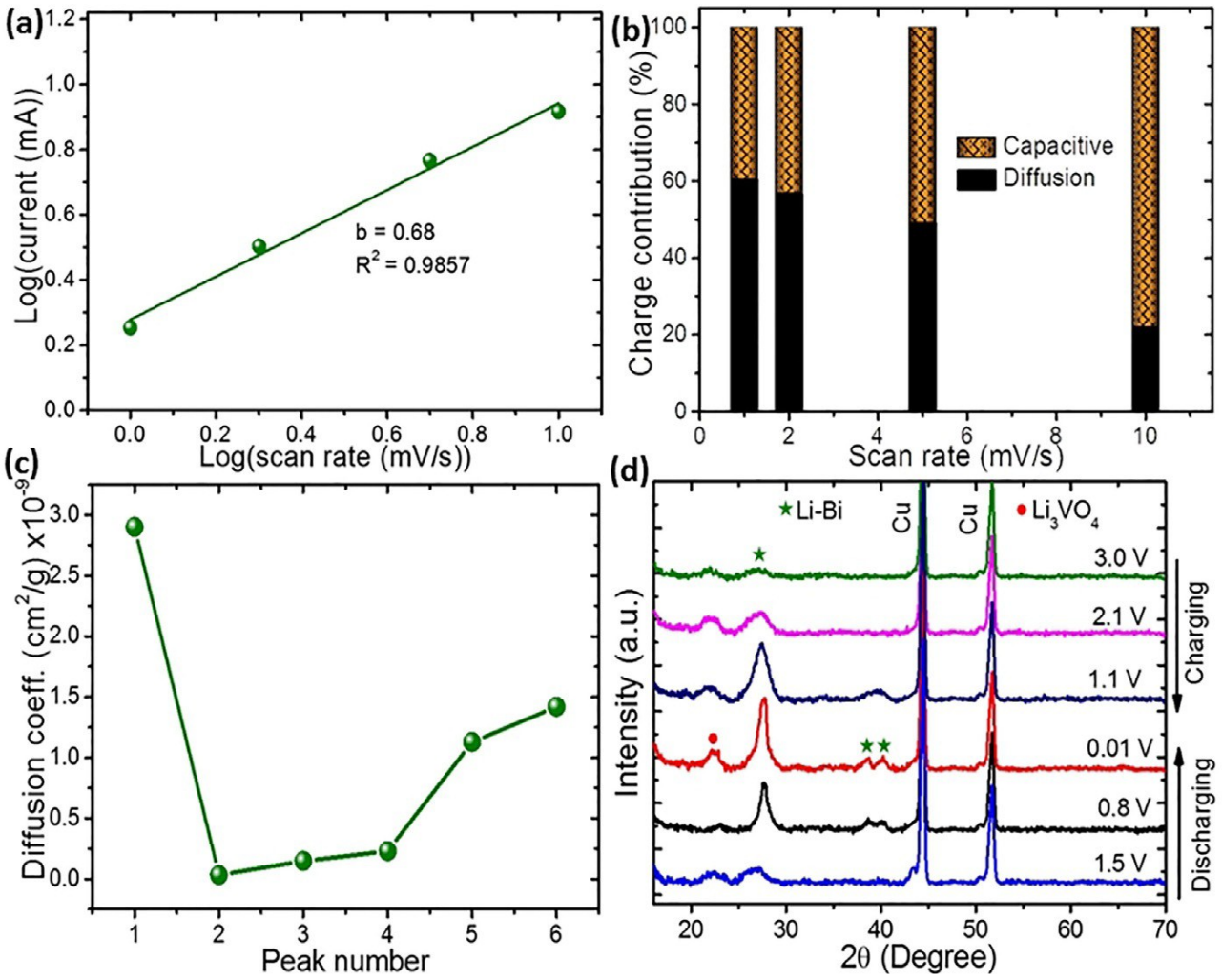

Figure 4. a) Plot of log (current) vs. log(scan rate) for cathodic responses. b) The contribution from capacitive and diffusion-controlled charge storage in BiVO4 electrode at different scan rates. c) Li-ion diffusion coefficients at different peak positions in CV curves measured at a scan rate of 1 mVs-1. d) Ex situ XRD patterns of electrodes at different charge and discharge potentials.

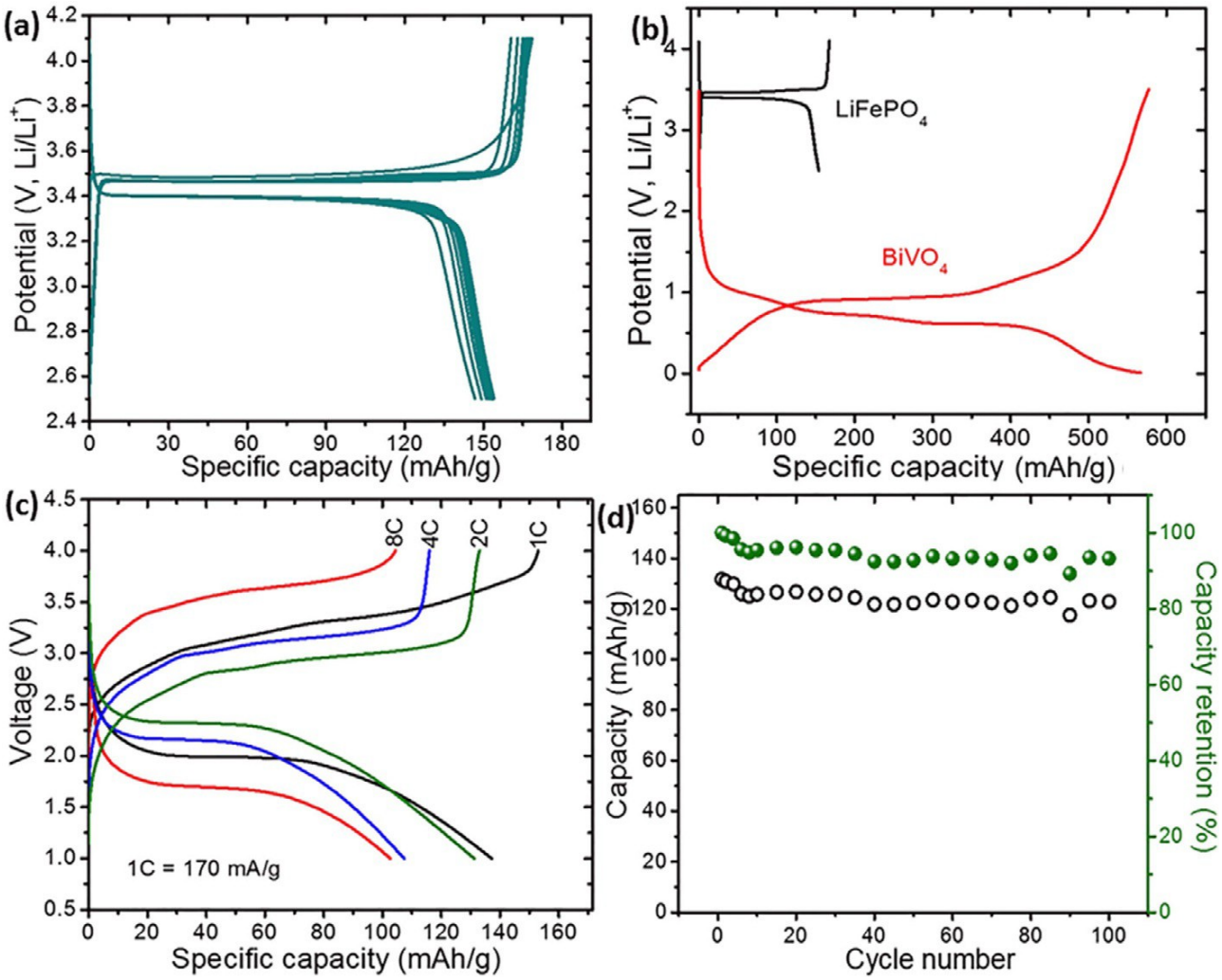

Figure 5. a) Charge-discharge (CD) curves for LiFePO4 (LFP) in half-cell configuration at 1C rate (1C=170 mAg-1). b) Comparative CD curves for LFP and BiVO4 in half-cell design. c) Charge–discharge profiles of a full cell composed of BiVO4 anode and LiFePO4 (LFP) cathode at various C rates. d) Variation of specific capacity and capacity retention at different CD cycles.